Applied Physics Letters

RESEARCH ARTICLE | FEBRUARY 12 2024

Electrical manipulation of dissipation in microwave photon–magnon hybrid system through the spin Hall effect

Special Collection: Magnonics

Justin T. Hou ; Chung-Tao Chou ; Jiahao Han ; Yabin Fan ; Luqiao Liu

Check for updates

Appl. Phys. Lett. 124, 072401 (2024)
https://doi.org/10.1063/5.0182270

View Online
Export Citation

26 August 2024 13:42:24

Nanotechnology & Materials Science
Optics & Photonics
Impedance Analysis
Scanning Probe Microscopy
Sensors
Failure Analysis & Semiconductors

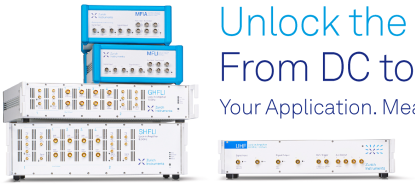

Unlock the Full Spectrum.
From DC to 8.5 GHz.
Your Application. Measured.

Find out more

Zurich Instruments

AIP Publishing

Applied Physics Letters ARTICLE pubs.aip.org/aip/apl

Electrical manipulation of dissipation in microwave photon–magnon hybrid system through the spin Hall effect

Cite as: Appl. Phys. Lett. **124**, 072401 (2024); doi: 10.1063/5.0182270
Submitted: 18 October 2023 · Accepted: 5 January 2024 ·
Published Online: 12 February 2024

Justin T. Hou,[1] Chung-Tao Chou,[2] Jiahao Han,[1] Yabin Fan,[1] and Luqiao Liu[1,a)]

AFFILIATIONS

[1]Department of Electrical Engineering and Computer Science, Massachusetts Institute of Technology, Cambridge, Massachusetts 02139, USA
[2]Department of Physics, Massachusetts Institute of Technology, Cambridge, Massachusetts 02139, USA

Note: This paper is part of the APL Special Collection on Magnonics.

[a)]**Author to whom correspondence should be addressed:** luqiao@mit.edu

ABSTRACT

Hybrid dynamic systems combine advantages from different subsystems for realizing information processing tasks in both classical and quantum domains. However, the lack of controlling knobs in tuning system parameters becomes a severe challenge in developing scalable, versatile hybrid systems for useful applications. Here, we report an on-chip microwave photon–magnon hybrid system where the dissipation rates and the coupling cooperativity can be electrically influenced by the spin Hall effect. Through magnon–photon coupling, the linewidths of the resonator photon mode and the hybridized magnon polariton modes are effectively changed by the spin injection into the magnetic wires from an applied direct current, which exhibit different trends in samples with low and high coupling strengths. Moreover, the linewidth modification by the spin Hall effect shows strong dependence on the detuning of the two subsystems, in contrast to the classical behavior of a standalone magnonic device. Our results point to a direction of realizing tunable, on-chip, scalable magnon-based hybrid dynamic systems, where spintronic effects provide useful control mechanisms.

© 2024 Author(s). All article content, except where otherwise noted, is licensed under a Creative Commons Attribution (CC BY) license (http://creativecommons.org/licenses/by/4.0/). https://doi.org/10.1063/5.0182270

26 August 2024 13:42:24

Hybrid dynamic systems combine two or more subsystems to achieve control, sensing, transduction, and information processing beyond the capability of each individual ones.[1,2] Tuning the properties of mutually interacted subsystems in a controllable way, including their frequencies, dissipation rates, and coupling strengths, lies at the center of developing functional hybrid systems. So far, various techniques have been developed for tuning the frequencies of hybrid systems, including varying the flux biases on superconducting qubits,[3] varying external magnetic fields for spin ensembles in paramagnetic materials[4,5] or magnons in ferromagnetic materials,[6–8] etc. Meanwhile, modulating the coupling strengths and dissipation rates represents more challenging tasks, with the former fixed by device geometries and requiring specialized circuits[9–11] and the later pre-determined by intrinsic material properties.

Magnon–photon hybrid systems have recently been implemented[12–22] in order to realize various critical functions, including signal isolations and frequency interconversions, by exploiting unique magnonic physics of frequency tunability,[23] time-reversal symmetry breaking,[24] dissipative coupling,[25–27] etc. Particularly, on-chip, lithographically defined magnon–photon structures with high cooperativities have been demonstrated,[6–8] opening up avenues for integrating functional magnetic components in large-scale circuits. Enabled by the on-chip nanoscale device design, various spintronic effects like spin torques[28–32] and voltage controlled magnetic anisotropy[33–35] can be potentially leveraged to control magnons, including their dissipations and frequencies. However, the requirements of both efficient spin current injections and high coupling strengths in a single device pose significant experimental challenges. To date, a microwave photon–magnon hybrid system with spin torque enabled tunable dissipation is yet to be demonstrated.

In this paper, we report an on-chip microwave photon–magnon hybrid system where the dissipation rates and the coupling cooperativity are influenced via an electrical current. Figure 1(a) illustrates the operating principle: inside a microwave resonator inductively coupled

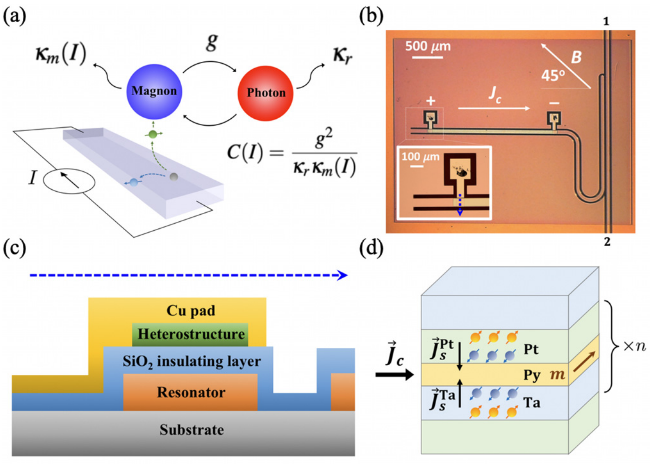

FIG. 1. (a) Schematic diagram showing a magnon–photon hybrid system where the magnon dissipation can be electrically adjusted by the spin Hall effect (SHE) using a direct current, thereby tuning the photon subsystem and the hybrid system cooperativity. (b) Microscope photo of a quarter-wave planar resonator with a $2\,\mathrm{mm} \times 52\,\mu\mathrm{m}$ $[\mathrm{Ta/Py/Pt}]_n$ stripe on top. The inset shows a current injection pad with the magnetic stripe. (c) Device cross section along the blue dashed line in (b). (d) Spin current injection into Py layers by the SHE in the magnetic heterostructure.

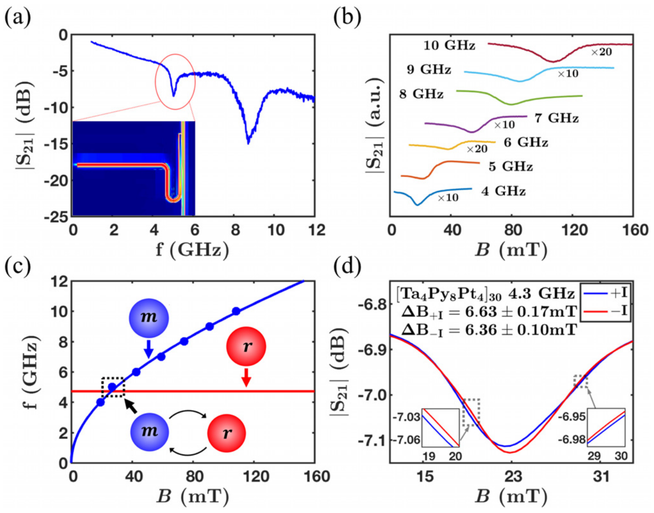

FIG. 2. (a) Microwave transmission of an unloaded quarter-wave resonator at room temperature. The inset shows the simulation of current density distribution of the fundamental mode, where red (blue) area represents regions with high (low) current densities. (b) Microwave transmission signals in a sample with $[\mathrm{Ta(4)/Py(8)/Pt(4)}]_{30}$ stripe. The spectra under certain frequencies are magnified by 10 or 20 times for displaying them on the same plot. To be comparable with the rest of the work, the magnetic resonance was measured under a current of $J_c = +9.6 \times 10^9\ \mathrm{A/m^2}$ flowing through the magnetic stripe. (c) Frequency vs applied field of ferromagnetic resonance, with the blue solid line representing fitting to the Kittel formula. The dashed square shows the field and frequency range focused on for the rest of our experiment, where the magnon (blue) and the resonator photon (red) modes are coupled. (d) Microwave transmission signals at 4.3 GHz under opposite current polarities.

with magnons, a charge current flowing through spin Hall effect (SHE) metals inject non-equilibrium spins into neighboring magnetic layers and change the magnon dissipation rate κ_m. This further influences the dissipations of hybridized magnon polariton modes and modulates the cooperativity. The current-induced linewidth modulation effects show strong dependence on the detuning and even exhibit different signs at different coupling regimes, which is distinct from isolated magnonic devices studied previously and reflects the coupled dynamics nature. Our results introduce SHE as a convenient *in situ* method for controlling hybridization between magnons and other quantum objects.

We utilize coplanar waveguide resonators to reach high magnon–photon coupling strengths.[6–8] Figure 1(b) shows an image of a quarter-wave resonator made of copper on a sapphire substrate defined through the combination of lithography and ion beam etching. Compared with superconducting resonators,[6–8] the utilization of normal metals removes the stringent requirement on operation temperature and provides a larger thermal budget. The side-coupled resonator is 2.5 μm thick, 60 μm wide, and 6 mm long, which results in a fundamental mode with resonant frequency $\omega_r/2\pi \approx 5\,\mathrm{GHz}$ and an unloaded quality factor of 18 at room temperature [Fig. 2(a)]. The fabricated Cu resonator is covered with a layer of 900 nm thick SiO$_2$ to avoid direct electrical contact between the resonator and the magnetic layers above. For the fundamental mode, the current distribution reaches a maximum at the shorted end of the resonator [inset of Fig. 2(a)], corresponding to the position with the strongest inductive coupling strength, where a $[\mathrm{Ta(4)/Permalloy(Py)}(t)\mathrm{/Pt(4)}]_n$ (units in nanometers) superlattice structure of 52 μm wide and 2 mm long is deposited, as shown by the light green color region in Fig. 1(b). To apply a direct current, Cu contact pads are connected onto the stripe [Figs. 1(b) and 1(c)], which are wire bonded to the leads of an external current source. The magnon–photon coupling strength g depends on the total spin numbers N_s through $g = g_s\sqrt{N_s}$, where g_s is single spin coupling strength as determined by the device geometry.[17,18] In order to examine the influence of SHE in systems with different couplings, two types of magnetic wires with different N_s are used in our experiment, corresponding to $(t, n) = (4, 15)$ and $(t, n) = (8, 30)$, respectively. Instead of using a single thick magnetic layer, we divide it into multiple repeats of thin individual layers to ensure that each Py layer is thin enough for efficient spin torque, and at the same time to achieve a high N_s for large coupling strength. Under an applied charge current, the heavy metals Ta and Pt with opposite spin Hall angles,[36–38] located at the opposite surfaces of the Py layer, will inject spins with the same polarization into Py through SHE [Fig. 1(d)]. The thicknesses of Pt (Ta) are chosen to be comparable to their spin diffusion lengths[39] for blocking spin flows in the unwanted directions and maximizing the spin Hall efficiency. During the measurement, an in-plane magnetic field B is applied at 45° angle with respect to the magnetic stripe [Fig. 1(b)] so that finite magnon–photon coupling and SHE-induced magnetic dissipation tuning can be reached simultaneously. The device is mounted in a cryostat and the microwave transmission coefficient S_{21} between port 1 and port 2 of the fabricated devices [Fig. 1(b)] is measured by a Vector Network Analyzer. Under the applied direct currents, the estimated device temperatures are 110 and 100 K for samples with $(t, n) = (4, 15)$ and $(t, n) = (8, 30)$, respectively, based on resistances of the heterostructure bars.

The S_{21} is first measured over a broad frequency to characterize the uniform magnon mode of the magnetic heterostructure. As an

26 August 2024 13:42:24

© Author(s) 2024

example, Fig. 2(b) shows the signals from the sample with a $[\mathrm{Ta}(4)/\mathrm{Py}(8)/\mathrm{Pt}(4)]_{30}$ stripe as a function of applied fields. Away from the resonator mode near 4.8 GHz, the signal represents ordinary ferromagnetic resonance (FMR), whose resonant frequencies and fields are summarized by blue dots in Fig. 2(c). The blue solid line represents fitting to the Kittel formula $\omega_m(B) = \gamma\sqrt{B(B+\mu_0 M_s)}$ with saturation magnetization $\mu_0 M_s = 1.0$ T and gyromagnetic ratio $\gamma/2\pi = 28$ GHz/T. At each frequency, we measure the resonance signals while applying direct currents with opposite polarities $\pm I$ onto the stripe. In Fig. 2(d), the magnon linewidth is larger under $+I$ than $-I$, consistent with SHE-induced magnetic damping change.[29,40] For the rest of the work, we focus on the hybrid system dynamics when the magnons and photons are near resonance, as denoted by the dashed square in Fig. 2(c).

When the frequencies of the magnon ω_m and the microwave resonator ω_r are close to each other, the resonance spectra are influenced by their mutual coupling. Figures 3(a) and 3(b) show microwave transmission signals of two resonators with $[\mathrm{Ta}(4)/\mathrm{Py}(4)/\mathrm{Pt}(4)]_{15}$ (sample 1) and $[\mathrm{Ta}(4)/\mathrm{Py}(8)/\mathrm{Pt}(4)]_{30}$ (sample 2) magnetic stripes, respectively, measured in the presence of applied direct currents. The magnon–photon coupling strengths are determined to be $g_1/2\pi = 98 \pm 3$ MHz and $g_2/2\pi = 268 \pm 7$ MHz for the two samples (discussed later). Moreover, we determine the dissipation rates (half width at half maximum, or HWHM) of magnon and resonator under applied currents independently, $\kappa_{m1}/2\pi = 495 \pm 4$ MHz and $\kappa_{r1}/2\pi = 53.2 \pm 1.2$ MHz for sample 1, and $\kappa_{m2}/2\pi = 592 \pm 9$ MHz and $\kappa_{r2}/2\pi = 110 \pm 1$ MHz for sample 2, based on the measurement away from the frequency crossing (see S1 of the supplementary material). With these parameters, the cooperativities for the two samples are calculated to be $C = g^2/\kappa_m\kappa_r = 0.39 \pm 0.02$ and 1.10 ± 0.05, respectively. Consistent with the low C in sample 1, Fig. 3(a) shows a simple crossing of the two modes, with frequencies of $\omega_{r1}/2\pi = 4.64$ GHz (red line) and $\omega_m(B)$ fitted well with the Kittel formula (blue line). Meanwhile, the larger C value of sample 2 leads to the appearance of mode anticrossing in Fig. 3(b). The two hybrid modes [purple and green branches in Fig. 3(b)] can be described by $\omega_\pm(B) = \omega_{r2} + \Delta(B)/2 \pm \sqrt{\Delta(B)^2 + 4g_2^2}/2$, where $\omega_{r2}/2\pi = 4.74$ GHz and $\Delta(B) = \omega_m(B) - \omega_r$ is the detuning between magnons and resonator photons.[7]

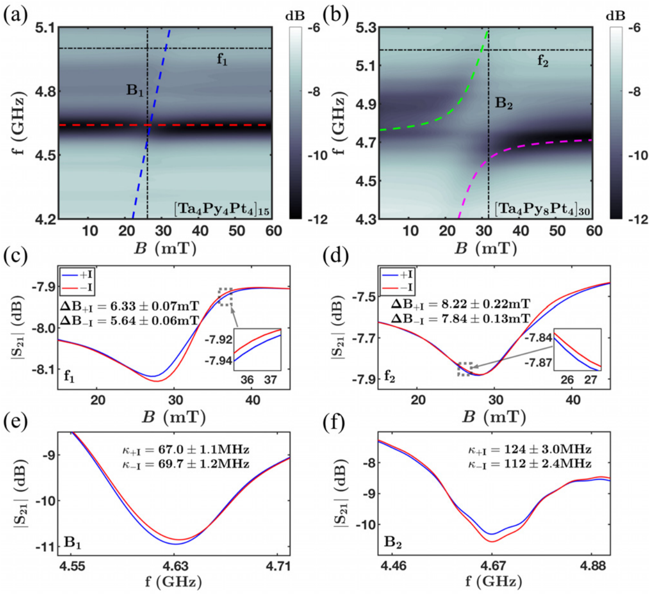

FIG. 3. (a), (c), and (e) are for sample 1 and (b), (d), and (f) are for sample 2. (a) and (b) Microwave transmission as a function of frequency and in-plane magnetic field. (c)–(f) Comparison of microwave transmission signals with opposite current polarities at a fixed frequency or applied field specified in (a) and (b). The data are measured under average charge current densities through the heterostructures $|\mathbf{J}_c| = 1.7 \times 10^{10}$ A/m^2 in sample 1 and $|\mathbf{J}_c| = 9.6 \times 10^9$ A/m^2 in sample 2, respectively. Results in (a) and (b) correspond to ones measured under positive currents.

We apply direct currents on magnetic stripes while measuring S_{21} spectra to inspect the influence of SHE onto the hybrid system dynamics. For sample 1, Figs. 3(c) and 3(e) shows the comparison of the transmission signals under $\pm I$ at a fixed frequency $f_1 = 5.00$ GHz or a fixed field $B_1 = 26$ mT [black lines in Fig. 3(a)]. First, with a large detuning at f_1 [Fig. 3(c)], we are observing the current's influence onto the pure magnon mode. The transmission spectra under $+I$ exhibit larger linewidth than $-I$, consistent with Fig. 2(d). On the other hand, with a small detuning [Fig. 3(e)], the resonator mode linewidth is decreased (increased) under a positive (negative) current, which is opposite to the trend for pure magnons in Fig. 2(c). This trend of the resonance linewidth change is also opposite to the changes observed in sample 2 with a higher cooperativity, where for both the fixed frequency [$f_2 = 5.18$ GHz, Fig. 3(d)] and fixed field traces [$B_2 = 32$ mT, Fig. 3(f)], the linewidth changes have the same sign with the pure magnon case. To check the robustness of the observed effects, we also measure the spectra by reversing the applied magnetic field directions and find that the current-induced linewidth change flips its sign in both samples, consistent with the SHE (see S8 of the supplementary material).

The two samples not only exhibit opposite signs in dissipation rate changes under applied currents, but also show distinct detuning dependences. Figure 4 illustrates the HWHM linewidth variations $\delta\kappa = (\kappa_{+\mathrm{I}} - \kappa_{-\mathrm{I}})/2$ as a function of applied fields, where $\kappa_{+\mathrm{I}}$ ($\kappa_{-\mathrm{I}}$) is the dissipation rate measured under $+I$ ($-I$). Here, we extract the influence of the SHE and avoid contributions from heating by

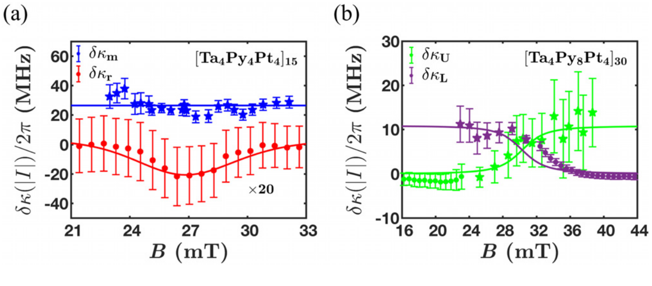

FIG. 4. (a) Current-induced linewidth modulation of magnon and resonator photon modes, $\delta\kappa_m$ and $\delta\kappa_r$, as a function of applied field in sample 1. To assist the visualization, $\delta\kappa_r$ (red dot and line) has been scaled by 20 times. (b) Current-induced linewidth modulation of the upper and lower branches $\delta\kappa_U$ and $\delta\kappa_L$ as a function of applied field in sample 2. A pentagram (circle) dot in (a) or (b) represents a data point obtained by a field (frequency) sweep at a fixed frequency (field), whose resonant field (frequency) is shown by the curves with the same color in Figs. 3(a) and 3(b) correspondingly.

26 August 2024 13:42:24

© Author(s) 2024

comparing the linewidths under ±I. For sample 1, the two distinct resonance modes are the magnon and resonator photon modes [blue and red dashed lines in Fig. 3(a)]. Correspondingly, $\delta\kappa_m$ remains nearly constant across the measured field range in Fig. 4(a) as expected from SHE-induced magnetic damping change, while $\delta\kappa_r$ shows a negative peak when the detuning of the two subsystems is small. The opposite signs in $\delta\kappa_m$ and $\delta\kappa_r$ demonstrate that SHE has opposite effects on the magnon and resonator linewidths in the coupled system with a low cooperativity. In sample 2, because of mode hybridization, the resonances separate into upper and lower branches [green and purple dashed lines in Fig. 3(b)], with the corresponding current-induced linewidth change shown in Fig. 4(b) (green and purple dots for $\delta\kappa_U$ and $\delta\kappa_L$ separately). Far away from the anticrossing, the detuning Δ is much larger than the coupling strength; therefore, the two modes remain at the isolated magnon and resonator photon modes, which accounts for the constant positive or zero values of $\delta\kappa_{m,r}$ at high and low fields. At zero detuning, the mutual coupling lifts up the degeneracy and leads to the formation of magnon polaritons $c_{U/L} = (a_m \pm a_r)/\sqrt{2}$ with a_m and a_r being the annihilation operators of magnons and resonator photons. Under this condition, the dissipation rate change caused by the SHE reaches one half of the pure magnon case, as reflected in the mid-field region of Fig. 4(b).

To quantitatively understand the SHE on the two samples with different cooperativities, we adopt the input–output theory, which describes the microwave transmission signal as a function of excitation frequency ω and applied magnetic field B:[41,42]

$$S_{21} = 1 - \frac{\kappa_{re}}{i(\omega_r - \omega) + \kappa_r + \dfrac{g^2}{i(\omega_m(B) - \omega) + \kappa_m(I)}}, \tag{1}$$

where κ_{re} is the coupling of the resonator to the external circuit. Under SHE, spins affect S_{21} of the hybrid system via modulating κ_m through $\delta\kappa_m(I) = \gamma \frac{\cos\theta}{\mu_0 M_s t_{\mathrm{FM}}} \frac{\hbar}{2e} (\Theta_{\mathrm{Pt}} J_c^{\mathrm{Pt}} + \Theta_{\mathrm{Ta}} J_c^{\mathrm{Ta}})$, with $\hbar$ and e representing the Planck's constant and electron charge, t_{FM} being the thickness of each Py layer, θ being the angle between magnetization and injected spin moments, Θ_{Pt}, Θ_{Ta}, J_c^{Pt}, J_c^{Ta} being the spin Hall angles and charge current densities of Pt and Ta layers,[40] where the latter two can be approximately determined using a parallel circuit model on the heterostructure of Fig. 1(d). The eigen frequencies and the effective dissipation rates as a function of I can be determined using the transfer function in Eq. (1). In the following, we discuss the approximate solutions applicable to samples 1 and 2 separately, with both cases satisfying $\kappa_m \gg \kappa_r$. For sample 1 with low coupling strength, the effective linewidth of the magnon mode is close to its intrinsic value $\kappa_{m,\mathrm{eff}}(I) \approx \kappa_m(I)$ (see S2 of the supplementary material), which is to the leading order not influenced by its coupling with the resonator. This is consistent with the constant $\delta\kappa_{m,\mathrm{eff}}(I)$ observed across the field range in Fig. 4(a). Using resistivities $\rho_{\mathrm{Pt}} = 12\ \mu\Omega\,\mathrm{cm}$, $\rho_{\mathrm{Py}} = 80\ \mu\Omega\,\mathrm{cm}$, and $\rho_{\mathrm{Ta}} = 180\ \mu\Omega\,\mathrm{cm}$,[36,43,44] and spin Hall angles $\Theta_{\mathrm{Pt}} = 0.3$[45] and $\Theta_{\mathrm{Ta}} = -0.2$,[46] we calculate $\delta\kappa_m(|I|)/2\pi = 27\,\mathrm{MHz}$, agreeing well with the experimental data [blue solid line in Fig. 4(a)]. Meanwhile, the dissipation rate of the resonator photon mode can be approximated as (see S2 of the supplementary material)

$$\kappa_{r,\mathrm{eff}}(I) \approx \kappa_r \left[1 + C(I) \frac{\kappa_m(I)^2}{\Delta^2 + \kappa_m(I)^2}\right]. \tag{2}$$

For the special case of zero detuning $\Delta = 0$, a simple relation follows: $\kappa_{r,\mathrm{eff}}(I) \approx \kappa_r[1 + C(I)]$, which is enhanced from the unloaded value by $C(I)$.[17] When $\kappa_m(I)$ increases under an applied current, the corresponding $C = g^2/\kappa_m\kappa_r$ decreases, resulting in a smaller $\kappa_{r,\mathrm{eff}}(I)$, which qualitatively explains the negative dip in the low detuning region of Fig. 4(a). Quantitatively, from Eq. (2), we get

$$\delta\kappa_{r,\mathrm{eff}}(|I|) = -g^2 \frac{\kappa_m^2 - \Delta^2}{(\kappa_m^2 + \Delta^2)^2} \times \delta\kappa_m(|I|). \tag{3}$$

The red line in Fig. 4(a) represents fitting using Eq. (3), where the single fitting parameter g is determined, $g/2\pi = 98 \pm 3\,\mathrm{MHz}$, reaching reasonable agreement with the estimated value of 108 MHz using the geometry of the resonator and the volume of the magnetic stripes.[7]

We now turn to the discussion of sample 2. First, for the strongly coupled system with $g \gg \kappa_m, \kappa_r$, it can be shown that the current-induced dissipation rate changes of the hybridized modes are $\delta\kappa_{U/L} = \cos^2\gamma_\pm \times \delta\kappa_m(|I|)$, where $(\cos\gamma_\pm \quad \sin\gamma_\pm)^T$ is the eigenstate of the hybrid system Hamiltonian $H = \omega_m a_m^\dagger a_m + \omega_r a_r^\dagger a_r + g(a_m^\dagger a_r + a_r^\dagger a_m)$ with $\cos^2\gamma_\pm = [1 \pm \Delta/\sqrt{\Delta^2 + 4g^2}]/2$ (see S2 of the supplementary material). The linear dependence of $\delta\kappa_{U/L}$ on $\delta\kappa_m(|I|)$ is consistent with the intuition that the dissipation change of the hybridized modes originates from its magnon portion whose magnitude is $\cos^2\gamma_\pm$. This analysis gives simple results $\delta\kappa_{U/L} \approx \delta\kappa_m$ or 0 when $|\Delta| \gg 2g$, and $\delta\kappa_{U/L} = \delta\kappa_m/2$ when $\Delta = 0$. In our sample, the condition of $g \gg \kappa_m, \kappa_r$ is not fully satisfied. However, one can show that a similar formula of $\delta\kappa_{U/L} = [1 \pm \Delta/\sqrt{\Delta^2 + 4g^2 - (\kappa_m - \kappa_r)^2}]/2 \times \delta\kappa_m(|I|)$ approximately describes the current's influence on dissipation rates, as represented by the green and purple solid lines in Fig. 4(b). Through the $\delta\kappa$ fitting, we determine $g/2\pi = 268 \pm 7\,\mathrm{MHz}$ for sample 2, consistent with the result obtained by fitting the two branches $\omega_\pm(B)$ in Fig. 3(b). The magnon dissipation $\kappa_m(I)/2\pi$ is electrically tunable and results in the current-induced cooperativity change ≈ 4%.

In summary, we experimentally investigated the influence of the SHE on magnon–photon hybrid system dissipation. The spin injection not only changes the magnon polaritons dissipation rates but also adjust the magnon–photon cooperativity $C(I) = g^2/\kappa_r\kappa_m(I)$. The current-induced cooperativity change can be further enhanced by scaling down the resonator channel width and using low damping magnetic material and high SHE alloys or topological materials.[47,48] Our discovery can provide a useful control mechanism for tuning the transduction between magnons and other quantum objects. Finally, by further tuning the dissipation rate to a negative value, we expect highly coherent self-oscillations through the spin–photon coupling, enabling an on-chip, electrically pumped spin-torque-oscillator maser device.[49]

See the supplementary material for device fabrication and measurement, derivations of SHE on hybrid system linewidths, simulations on resonators, transmission signals with opposite field polarities, varied detunings, and different current magnitudes.

The work was supported by AFOSR under Grant No. FA9550-19-1-0048 and the National Science Foundation under Grant No.

26 August 2024 13:42:24

© Author(s) 2024

ECCS-2309838. J.T.H. thanks P.-C. Shih for discussion on the TEOS-PECVD deposition.

AUTHOR DECLARATIONS

Conflict of Interest

J.T.H and L.L. have U.S. Patent Application No. 18/193,885 pending.

Author Contributions

Justin T. Hou: Conceptualization (equal); Formal analysis (equal); Investigation (equal); Project administration (equal); Validation (equal); Writing – original draft (equal); Writing – review & editing (equal). **Chung-Tao Chou:** Investigation (supporting); Writing – review & editing (supporting). **Jiahao Han:** Investigation (supporting); Writing – review & editing (supporting). **Yabin Fan:** Investigation (supporting); Writing – review & editing (supporting). **Luqiao Liu:** Conceptualization (equal); Funding acquisition (equal); Project administration (equal); Supervision (equal); Writing – review & editing (equal).

DATA AVAILABILITY

The data that support the findings of this study are available from the corresponding author upon reasonable request.

REFERENCES

[1] Z.-L. Xiang, S. Ashhab, J. Q. You, and F. Nori, "Hybrid quantum circuits: Superconducting circuits interacting with other quantum systems," Rev. Mod. Phys. **85**, 623–653 (2013).

[2] G. Kurizki, P. Bertet, Y. Kubo, K. Mølmer, D. Petrosyan, P. Rabl, and J. Schmiedmayer, "Quantum technologies with hybrid systems," Proc. Natl. Acad. Sci. U. S. A. **112**, 3866–3873 (2015).

[3] A. Wallraff, D. I. Schuster, A. Blais, L. Frunzio, R.-S. Huang, J. Majer, S. Kumar, S. M. Girvin, and R. J. Schoelkopf, "Strong coupling of a single photon to a superconducting qubit using circuit quantum electrodynamics," Nature **431**, 162–167 (2004).

[4] Y. Kubo, F. R. Ong, P. Bertet, D. Vion, V. Jacques, D. Zheng, A. Dréau, J.-F. Roch, A. Auffeves, F. Jelezko, J. Wrachtrup, M. F. Barthe, P. Bergonzo, and D. Esteve, "Strong coupling of a spin ensemble to a superconducting resonator," Phys. Rev. Lett. **105**, 140502 (2010).

[5] D. I. Schuster, A. P. Sears, E. Ginossar, L. DiCarlo, L. Frunzio, J. J. L. Morton, H. Wu, G. A. D. Briggs, B. B. Buckley, D. D. Awschalom, and R. J. Schoelkopf, "High-cooperativity coupling of electron-spin ensembles to superconducting cavities," Phys. Rev. Lett. **105**, 140501 (2010).

[6] Y. Li, T. Polakovic, Y.-L. Wang, J. Xu, S. Lendinez, Z. Zhang, J. Ding, T. Khaire, H. Saglam, R. Divan, J. Pearson, W.-K. Kwok, Z. Xiao, V. Novosad, A. Hoffmann, and W. Zhang, "Strong coupling between magnons and microwave photons in on-chip ferromagnet-superconductor thin-film devices," Phys. Rev. Lett. **123**, 107701 (2019).

[7] J. T. Hou and L. Liu, "Strong coupling between microwave photons and nanomagnet magnons," Phys. Rev. Lett. **123**, 107702 (2019).

[8] I. Haygood, M. Pufall, E. Edwards, J. M. Shaw, and W. Rippard, "Strong coupling of an Fe-Co alloy with ultralow damping to superconducting Co-planar waveguide resonators," Phys. Rev. Appl. **15**, 054021 (2021).

[9] T. Hime, P. A. Reichardt, B. L. T. Plourde, T. L. Robertson, C.-E. Wu, A. V. Ustinov, and J. Clarke, "Solid-state qubits with current-controlled coupling," Science **314**, 1427 (2006).

[10] A. O. Niskanen, K. Harrabi, F. Yoshihara, Y. Nakamura, S. Lloyd, and J. S. Tsai, "Quantum coherent tunable coupling of superconducting qubits," Science **316**, 723 (2007).

[11] R. C. Bialczak, M. Ansmann, M. Hofheinz, M. Lenander, E. Lucero, M. Neeley, A. D. O'Connell, D. Sank, H. Wang, M. Weides, J. Wenner, T. Yamamoto, A. N. Cleland, and J. M. Martinis, "Fast tunable coupler for superconducting qubits," Phys. Rev. Lett. **106**, 060501 (2011).

[12] D. Lachance-Quirion, Y. Tabuchi, A. Gloppe, K. Usami, and Y. Nakamura, "Hybrid quantum systems based on magnonics," Appl. Phys. Express **12**, 070101 (2019).

[13] Y. Li, W. Zhang, V. Tyberkevych, W.-K. Kwok, A. Hoffmann, and V. Novosad, "Hybrid magnonics: Physics, circuits, and applications for coherent information processing," J. Appl. Phys. **128**, 130902 (2020).

[14] D. D. Awschalom, C. R. Du, R. He, F. J. Heremans, A. Hoffmann, J. Hou, H. Kurebayashi, Y. Li, L. Liu, V. Novosad, J. Sklenar, S. E. Sullivan, D. Sun, H. Tang, V. Tyberkevych, C. Trevillian, A. W. Tsen, L. R. Weiss, W. Zhang, X. Zhang, L. Zhao, and C. W. Zollitsch, "Quantum engineering with hybrid magnonic systems and materials (invited paper)," IEEE Trans. Quantum Eng. **2**, 5500836 (2021).

[15] Ö. O. Soykal and M. E. Flatté, "Strong field interactions between a nanomagnet and a photonic cavity," Phys. Rev. Lett. **104**, 077202 (2010).

[16] H. Huebl, C. W. Zollitsch, J. Lotze, F. Hocke, M. Greifenstein, A. Marx, R. Gross, and S. T. B. Goennenwein, "High cooperativity in coupled microwave resonator ferrimagnetic insulator hybrids," Phys. Rev. Lett. **111**, 127003 (2013).

[17] X. Zhang, C.-L. Zou, L. Jiang, and H. X. Tang, "Strongly coupled magnons and cavity microwave photons," Phys. Rev. Lett. **113**, 156401 (2014).

[18] Y. Tabuchi, S. Ishino, T. Ishikawa, R. Yamazaki, K. Usami, and Y. Nakamura, "Hybridizing ferromagnetic magnons and microwave photons in the quantum limit," Phys. Rev. Lett. **113**, 083603 (2014).

[19] L. Bai, M. Harder, Y. P. Chen, X. Fan, J. Q. Xiao, and C.-M. Hu, "Spin pumping in electrodynamically coupled magnon-photon systems," Phys. Rev. Lett. **114**, 227201 (2015).

[20] Y. Tabuchi, S. Ishino, A. Noguchi, T. Ishikawa, R. Yamazaki, K. Usami, and Y. Nakamura, "Coherent coupling between a ferromagnetic magnon and a superconducting qubit," Science **349**, 405–408 (2015).

[21] B. Bhoi, B. Kim, S.-H. Jang, J. Kim, J. Yang, Y.-J. Cho, and S.-K. Kim, "Abnormal anticrossing effect in photon-magnon coupling," Phys. Rev. B **99**, 134426 (2019).

[22] L. Bai, M. Harder, P. Hyde, Z. Zhang, C.-M. Hu, Y. Chen, and J. Q. Xiao, "Cavity mediated manipulation of distant spin currents using a cavity-magnon-polariton," Phys. Rev. Lett. **118**, 217201 (2017).

[23] J. Xu, C. Zhong, X. Han, D. Jin, L. Jiang, and X. Zhang, "Floquet cavity electromagnonics," Phys. Rev. Lett. **125**, 237201 (2020).

[24] X. Zhang, A. Galda, X. Han, D. Jin, and V. M. Vinokur, "Broadband nonreciprocity enabled by strong coupling of magnons and microwave photons," Phys. Rev. Appl. **13**, 044039 (2020).

[25] W. Yu, J. Wang, H. Y. Yuan, and J. Xiao, "Prediction of attractive level crossing via a dissipative mode," Phys. Rev. Lett. **123**, 227201 (2019).

[26] Y.-P. Wang, J. Rao, Y. Yang, P.-C. Xu, Y. Gui, B. Yao, J. You, and C.-M. Hu, "Nonreciprocity and unidirectional invisibility in cavity magnonics," Phys. Rev. Lett. **123**, 127202 (2019).

[27] M. Harder, Y. Yang, B. Yao, C. Yu, J. Rao, Y. Gui, R. Stamps, and C.-M. Hu, "Level attraction due to dissipative magnon-photon coupling," Phys. Rev. Lett. **121**, 137203 (2018).

[28] S. I. Kiselev, J. C. Sankey, I. N. Krivorotov, N. C. Emley, R. J. Schoelkopf, R. A. Buhrman, and D. C. Ralph, "Microwave oscillations of a nanomagnet driven by a spin-polarized current," Nature **425**, 380–383 (2003).

[29] K. Ando, S. Takahashi, K. Harii, K. Sasage, J. Ieda, S. Maekawa, and E. Saitoh, "Electric manipulation of spin relaxation using the spin Hall effect," Phys. Rev. Lett. **101**, 036601 (2008).

[30] V. E. Demidov, S. Urazhdin, E. R. J. Edwards, M. D. Stiles, R. D. McMichael, and S. O. Demokritov, "Control of magnetic fluctuations by spin current," Phys. Rev. Lett. **107**, 107204 (2011).

[31] V. E. Demidov, S. Urazhdin, H. Ulrichs, V. Tiberkevich, A. Slavin, D. Baither, G. Schmitz, and S. O. Demokritov, "Magnetic nano-oscillator driven by pure spin current," Nat. Mater. **11**, 1028–1031 (2012).

[32] L. Liu, C.-F. Pai, D. C. Ralph, and R. A. Buhrman, "Magnetic oscillations driven by the spin Hall effect in 3-terminal magnetic tunnel junction devices," Phys. Rev. Lett. **109**, 186602 (2012).

26 August 2024 13:42:24

© Author(s) 2024

[33] P. K. Amiri and K. L. Wang, "Voltage-controlled magnetic anisotropy in spintronic devices," SPIN **2**, 1240002 (2012).

[34] T. Maruyama, Y. Shiota, T. Nozaki, K. Ohta, N. Toda, M. Mizuguchi, A. A. Tulapurkar, T. Shinjo, M. Shiraishi, S. Mizukami, Y. Ando, and Y. Suzuki, "Large voltage-induced magnetic anisotropy change in a few atomic layers of iron," Nat. Nanotechnol. **4**, 158–161 (2009).

[35] B. Rana, Y. Fukuma, K. Miura, H. Takahashi, and Y. Otani, "Excitation of coherent propagating spin waves in ultrathin CoFeB film by voltage-controlled magnetic anisotropy," Appl. Phys. Lett. **111**, 052404 (2017).

[36] M. Morota, Y. Niimi, K. Ohnishi, D. H. Wei, T. Tanaka, H. Kontani, T. Kimura, and Y. Otani, "Indication of intrinsic spin Hall effect in 4*d* and 5*d* transition metals," Phys. Rev. B **83**, 174405 (2011).

[37] T. Tanaka, H. Kontani, M. Naito, T. Naito, D. S. Hirashima, K. Yamada, and J. Inoue, "Intrinsic spin Hall effect and orbital Hall effect in 4*d* and 5*d* transition metals," Phys. Rev. B **77**, 165117 (2008).

[38] G. Y. Guo, S. Murakami, T.-W. Chen, and N. Nagaosa, "Intrinsic spin Hall effect in platinum: First-principles calculations," Phys. Rev. Lett. **100**, 096401 (2008).

[39] X. Tao, Q. Liu, B. Miao, R. Yu, Z. Feng, L. Sun, B. You, J. Du, K. Chen, S. Zhang, L. Zhang, Z. Yuan, D. Wu, and H. Ding, "Self-consistent determination of spin Hall angle and spin diffusion length in Pt and Pd: The role of the interface spin loss," Sci. Adv. **4**, eaat1670 (2018).

[40] L. Liu, T. Moriyama, D. C. Ralph, and R. A. Buhrman, "Spin-torque ferromagnetic resonance induced by the spin Hall effect," Phys. Rev. Lett. **106**, 036601 (2011).

[41] C. W. Gardiner and M. J. Collett, "Input and output in damped quantum systems: Quantum stochastic differential equations and the master equation," Phys. Rev. A **31**, 3761–3774 (1985).

[42] N. Zhu, X. Han, C.-L. Zou, M. Xu, and H. X. Tang, "Magnon-photon strong coupling for tunable microwave circulators," Phys. Rev. A **101**, 043842 (2020).

[43] E. Sagasta, Y. Omori, M. Isasa, Y. Otani, L. E. Hueso, and F. Casanova, "Spin diffusion length of Permalloy using spin absorption in lateral spin valves," Appl. Phys. Lett. **111**, 082407 (2017).

[44] N. Schwartz, W. A. Reed, P. Polash, and M. H. Read, "Temperature coefficient of resistance of beta-tantalum films and mixtures with b.c.c.-tantalum," Thin Solid Films **14**, 333–346 (1972).

[45] C.-F. Pai, Y. Ou, L. H. Vilela-Leão, D. C. Ralph, and R. A. Buhrman, "Dependence of the efficiency of spin Hall torque on the transparency of Pt/ferromagnetic layer interfaces," Phys. Rev. B **92**, 064426 (2015).

[46] M. Cecot, L. Karwacki, W. Skowroński, J. Kanak, J. Wrona, A. Żywczak, L. Yao, S. van Dijken, J. Barnaś, and T. Stobiecki, "Influence of intermixing at the Ta/CoFeB interface on spin Hall angle in Ta/CoFeB/MgO heterostructures," Sci. Rep. **7**, 968 (2017).

[47] Q. Shao, P. Li, L. Liu, H. Yang, S. Fukami, A. Razavi, H. Wu, K. Wang, F. Freimuth, Y. Mokrousov, M. D. Stiles, S. Emori, A. Hoffmann, J. Åkerman, K. Roy, J.-P. Wang, S.-H. Yang, K. Garello, and W. Zhang, "Roadmap of spin orbit torques," IEEE Trans. Magn. **57**, 1–39 (2021).

[48] S. Emori, A. Matyushov, H.-M. Jeon, C. J. Babroski, T. Nan, A. M. Belkessam, J. G. Jones, M. E. McConney, G. J. Brown, B. M. Howe, and N. X. Sun, "Spin-orbit torque and spin pumping in YIG/Pt with interfacial insertion layers," Appl. Phys. Lett. **112**, 182406 (2018).

[49] J. T. Hou, P. Zhang, and L. Liu, "Proposal for a spin-torque-oscillator maser enabled by microwave photon-spin coupling," Phys. Rev. Appl. **16**, 034034 (2021).

26 August 2024 13:42:24

© Author(s) 2024